doi:10.1038/nature17430

A pressure-amplifying framework material with negative gas adsorption transitions

Simon Krause[1]*, Volodymyr Bon[1]*, Irena Senkovska[1], Ulrich Stoeck[1]†, Dirk Wallacher[2], Daniel M. Többens[3], Stefan Zander[3], Renjith S. Pillai[4], Guillaume Maurin[4], François-Xavier Coudert[5] & Stefan Kaskel[1]

Adsorption-based phenomena are important in gas separations[1,2], such as the treatment of greenhouse-gas[3] and toxic-gas[4] pollutants, and in water-adsorption-based heat pumps[5] for solar cooling systems. The ability to tune the pore size, shape and functionality of crystalline porous coordination polymers—or metal–organic frameworks (MOFs)—has made them attractive materials for such adsorption-based applications[3,6–8]. The flexibility and guest-molecule-dependent response[9,10] of MOFs give rise to unexpected and often desirable adsorption phenomena[11–14]. Common to all isothermal gas adsorption phenomena, however, is increased gas uptake with increased pressure. Here we report adsorption transitions in the isotherms of a MOF (DUT-49) that exhibits a negative gas adsorption; that is, spontaneous desorption of gas (methane and *n*-butane) occurs during pressure increase in a defined temperature and pressure range. A combination of *in situ* powder X-ray diffraction, gas adsorption experiments and simulations shows that this adsorption behaviour is controlled by a sudden hysteretic structural deformation and pore contraction of the MOF, which releases guest molecules. These findings may enable technologies using frameworks capable of negative gas adsorption for pressure amplification in micro- and macroscopic system engineering. Negative gas adsorption extends the series of counterintuitive phenomena such as negative thermal expansion[15,16] and negative refractive indices[17] and may be interpreted as an adsorptive analogue of force-amplifying negative compressibility transitions proposed for metamaterials[18].

In MOFs, guest-molecule-assisted phenomena, such as ligand flip[19], gating[20], and breathing[21,22] of the framework lead to adsorption isotherms with an S-shape, wide hysteresis and multiple steps[23], which give rise to previously unattainable potential applications[10]. As a general rule of thermodynamics, at constant temperature the absolute amount of substance in the adsorbed phase (n_{ads}) always increases with increasing pressure of the adsorptive (p), resulting in a positive slope (see equation (1)) in a single-component adsorption isotherm (Fig. 1a)[24]:

$$(\mathrm{d}n_{\mathrm{ads}}/\mathrm{d}p) \geq 0 \qquad (1)$$

However, here we describe a material with a negative gas adsorption (NGA) step, causing an unexpected pressure amplification triggered by a sudden structural transition of a nanoporous framework. We show that this phenomenon is observed upon adsorption of various gas molecules at characteristic temperature and pressure in DUT-49 (Dresden University of Technology No. 49), a framework with very high porosity. Initially, DUT-49 was discovered as a high-performance methane (CH_4) storage material for natural gas vehicles[25]. Its extremely high excess methane storage capacity of 308 g kg^{-1} at 110 bar and 298 K motivated us to elucidate the adsorption mechanism at lower temperatures. However, a methane adsorption isotherm recorded at 111 K revealed a peculiar drop that was originally regarded as an instrumental failure (Fig. 1b). Repeated isotherm measurements at 111 K gave evidence of a perfectly reproducible negative adsorption step around 10 kPa, strongly deviating from the previously reported adsorption profile at 298 K (up to 110 bar). With a drop of $\Delta n_{\mathrm{NGA}} = -8.62$ mmol g^{-1} the NGA step alone surpasses the adsorption capacity of commercially available nanoparticles and even of some zeolites[26]. Thus in volumetric adsorption experiments it causes a massive response and pressure amplification of $\Delta p_{\mathrm{NGA}} = 2.27$ kPa in the measuring cell (Fig. 1f), in contrast to what happens in any rigid microporous solids (Fig. 1e). This corresponds to a specific Δp_{NGA} for methane adsorption at 111 K of up to 493 kPa g^{-1} (Supplementary Table 1).

Additional adsorption experiments using *n*-butane at 298 K lead to a distinct NGA step at 30 kPa (Fig. 1c) with a kinetic profile (Fig. 1g) similar to that of methane (111 K) while isotherms of N_2 at 77 K (Supplementary Fig. 5) show a typical 'type I' slope, illustrating the subtle role of the gaseous guest molecule (N_2 in contrast to CH_4 and C_4H_{10}) and its specific interaction stimulating NGA in DUT-49. Gravimetric adsorption experiments with *n*-butane at 298 K in parallel with dynamic scanning calorimetry support the results obtained from volumetric adsorption experiments and also reveal a complex combination of exothermic and endothermic processes during NGA (Fig. 1d, Supplementary Fig. 24). In particular, exposing samples of DUT-49 to *n*-butane permits us to investigate NGA at room temperature below 100 kPa, conditions that are easily attained in a standard laboratory environment. Visual monitoring of the sample during the adsorption experiment reveals macroscopic movement of the particle ensemble caused by the massive gas release during NGA, followed by a pronounced shrinkage, by about 20%, of the packed bed volume (Fig. 1h, Supplementary Video 1). From this macroscopic observation we suspected NGA to be related to massive structural transformations in the crystalline solid. Real-time parallelized adsorption/diffraction/EXAFS (extended X-ray absorption fine structure) experiments carried out at the BESSY II light source at the Helmholtz-Zentrum Berlin using an improved setup[27] allowed us to elucidate the structural transformations *in situ*.

Synchrotron powder X-ray diffraction (PXRD) data collected during methane adsorption at 111 K indicate two distinct structural transitions of the open-pore structure DUT-49*op* at 10 kPa and 45–65 kPa correlating with the steps in the isotherm (Fig. 2a and b). DUT-49*op* is an assembly of cuboctahedral metal–organic polyhedra (MOPs) formed by Cu_2 paddle-wheel units and 9*H*-carbazole-3,6-dicarboxylates connected by biphenylene units resulting in face-centred cubic analogue arrangement of MOPs (a framework with **fcu** topology)[25]. Wide open voids (10 Å, 17 Å and 24 Å) originate from an ordered arrangement of MOPs, an expanded analogue of a cubic close packing of atoms

---

[1]Department of Inorganic Chemistry, Technische Universität Dresden, Bergstrasse 66, 01062 Dresden, Germany. [2]Department Sample Environments, Helmholtz-Zentrum Berlin für Materialien und Energie, Hahn-Meitner-Platz 1, 14109 Berlin, Germany. [3]Department Structure and Dynamics of Energy Materials, Helmholtz-Zentrum Berlin für Materialien und Energie, Hahn-Meitner-Platz 1, 14109 Berlin, Germany. [4]Institut Charles Gerhardt Montpellier UMR 5253 CNRS UM ENSCM, Université Montpellier, Place E. Bataillon, 34095 Montpellier cedex 05, France. [5]Chimie ParisTech, PSL Research University, CNRS, Institut de Recherche de Chimie Paris, 75005 Paris, France. †Present address: Institute for Complex Materials, Leibniz Institute for Solid State and Materials Research (IFW) Dresden, Helmholtzstraße 20, D-01069 Dresden, Germany.

*These authors contributed equally to this work.

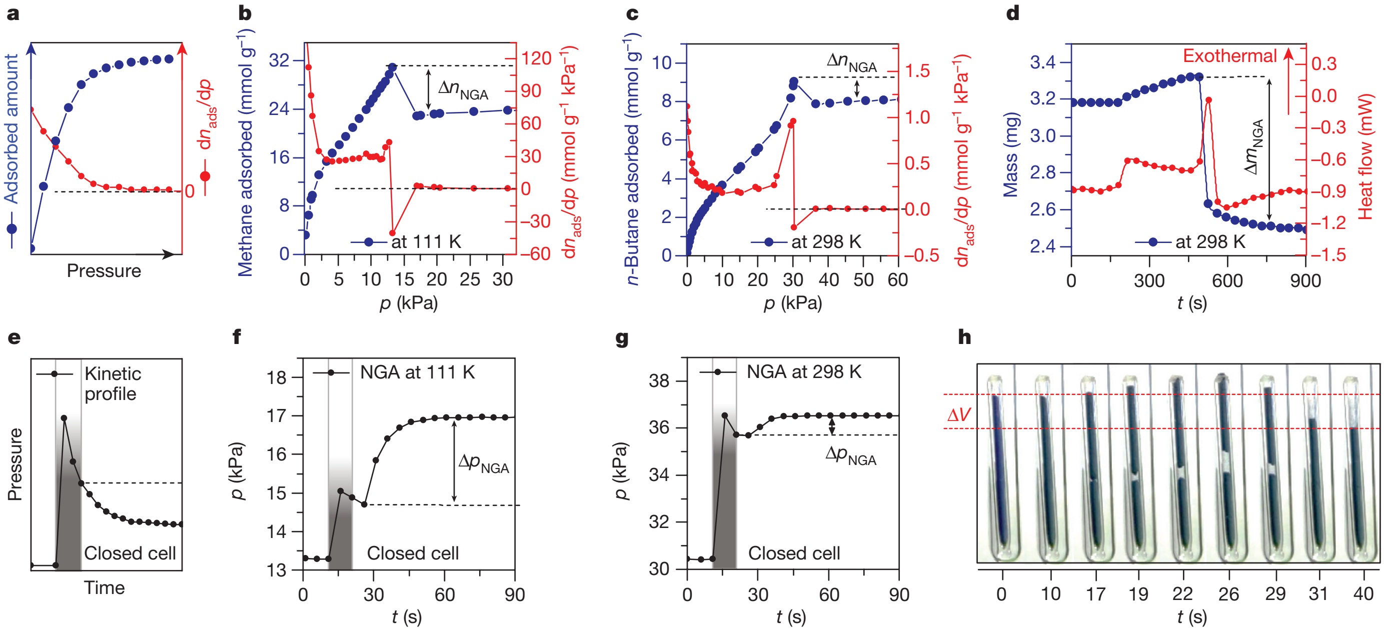

Figure 1 | Gas adsorption isotherms, pressure and kinetic profiles. **a**, Typical profile of type I adsorption isotherms for a non-breathing microporous solid and corresponding dn_{ads}/dp (ref. 24). **b**, **c**, Adsorption isotherms (blue) and corresponding derivatives (red) of DUT-49 for methane at 111 K (**b**) and n-butane at 298 K (**c**). Δn_{NGA} represents the NGA step in the isotherm. **d**, Gravimetric adsorption in parallel with dynamic scanning calorimetry, Δm_{NGA} represents the mass of the gas released during NGA. **e**–**g**, Corresponding kinetic pressure profiles for the typical adsorption behaviour of a non-breathing microporous solid (**e**), and for DUT-49 observed during the NGA step for methane at 111 K (**f**) and n-butane at 298 K (**g**); grey areas indicate the gas dosing interval. **h**, Snapshots of Supplementary Video 1 recorded during the n-butane adsorption steps at 298 K (**c**, **g**) (the capillary diameter is 1 mm and the sample bed is 5 cm in height at time $t = 0$ s).

but with huge tetrahedral and octahedral voids (Fig. 3a–c). During NGA the highly porous framework undergoes an enormous contraction of the unit cell volume from $V = 100{,}072$ Å^3 (calculated density $\rho_{calc} = 0.287$ g cm^{-3}) to a highly squeezed intermediate, the contracted-pore structure DUT-49*cp* with a unit cell volume of only 47,282 Å^3 ($\rho_{calc} = 0.661$ g cm^{-3}) (Supplementary Fig. 34), corresponding to a unit cell change in volume of more than 50,000 Å^3 (Fig. 2c). This initial transformation is reversible: as the pores become completely filled, expansion back to the original DUT-49*op* is observed (Supplementary Fig. 35).

From a structural point of view the contraction originates from concerted rotation of the MOPs around the threefold [111] axis leading to a severe deformation of the ligand (Fig. 3e, Supplementary Video 2). Yet the connectivity of the framework is preserved during the transformation and the porosity of the MOPs (pore diameter 10.1–9.9 Å) is only slightly affected. EXAFS spectra collected *in situ* during methane adsorption at 111 K confirm the unaltered coordination environment of Cu^{2+} (Supplementary Figs 38 and 39, Supplementary Table 8). In contrast, the pore diameter of the tetrahedral voids is reduced from 16.9 Å to 10.6 Å and the mesoporous octahedral voids deform even more, from

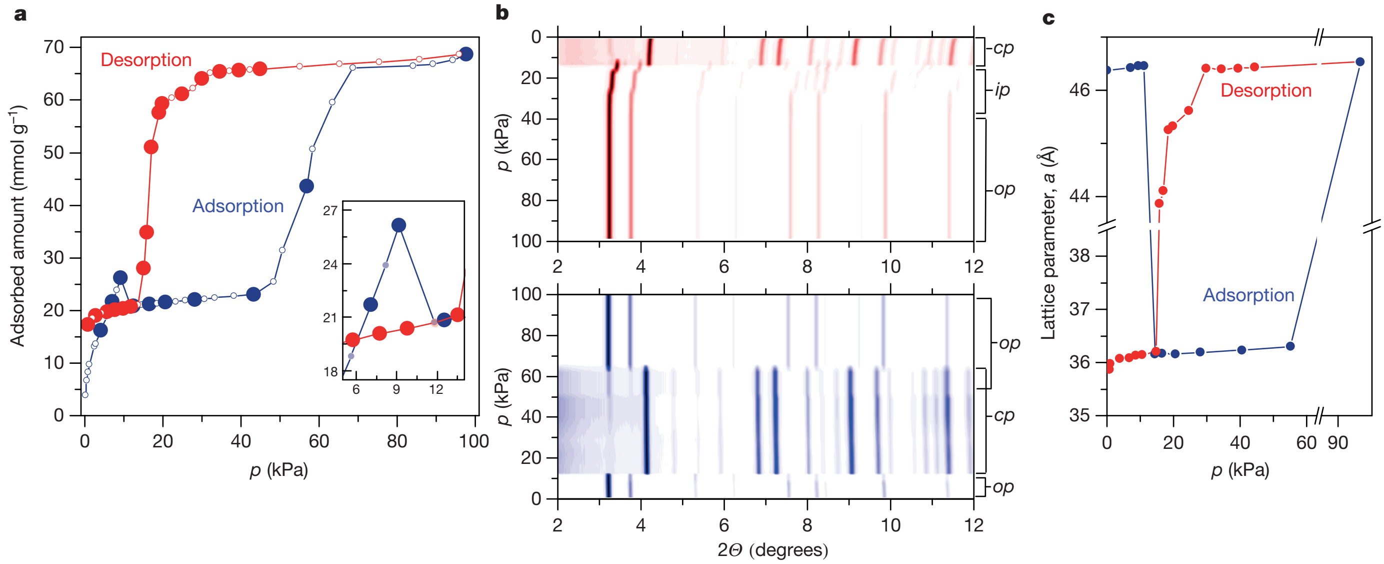

Figure 2 | *In situ* PXRD during methane adsorption at 111 K. **a**, Methane adsorption and desorption isotherms at 111 K collected *in situ*. The points corresponding to collected PXRD patterns are represented as solid symbols; the inset shows an enlarged NGA region of the isotherm. **b**, Contour plot of the PXRD pattern evolution ($\lambda = 1.5406$ Å) during adsorption (blue) and desorption (red). *op* is the open-pore phase (cubic, space group $F23$, lattice parameter $a = 46.427(4)$ Å), *cp* is the contracted-pore phase (cubic, $Pa\bar{3}$, $a = 36.1603(2)$ Å), and *ip* is the intermediate pore phase (cubic, $Pa\bar{3}$, $a = 45.542(2)$ Å). **c**, Lattice parameter evolution during adsorption (blue) and desorption (red) of methane at 111 K.

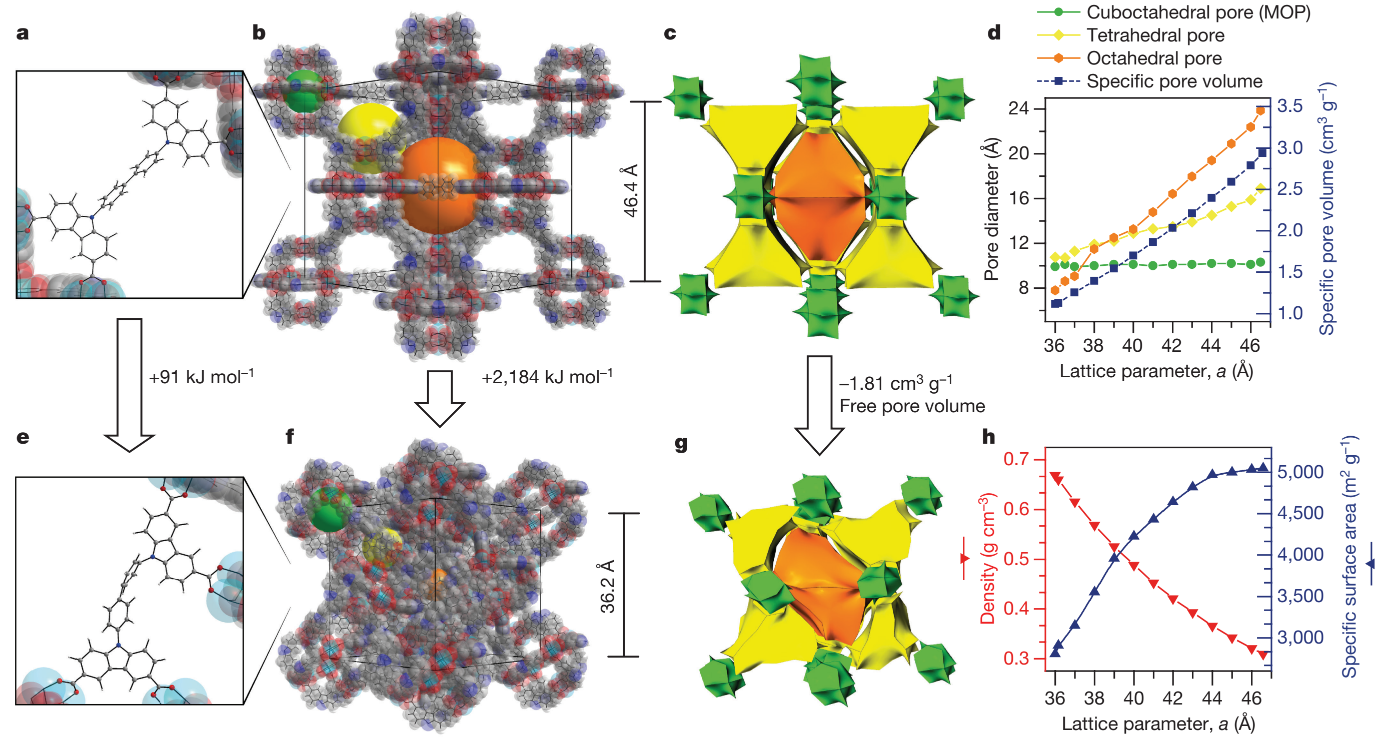

Figure 3 | Structure of DUT-49*op* and DUT-49*cp*. **a**, **e**, Conformation of 9,9′-([1,1′-biphenyl]-4,4′-diyl)bis(9*H*-carbazole-3,6-dicarboxylate) in DUT-49*op* (**a**) and DUT-49*cp* (**e**). **b**, **f**, View of the crystal structure along [110] for DUT-49*op* (simulated accessible surface area 5,049 $\mathrm{m^2\ g^{-1}}$, free pore volume 2.94 $\mathrm{cm^3\ g^{-1}}$) (**b**) and DUT-49*cp* (simulated accessible surface area 2,908 $\mathrm{m^2\ g^{-1}}$, free pore volume 1.13 $\mathrm{cm^3\ g^{-1}}$) (**f**). Atoms are coloured as follows: C (dark grey), N (blue), O (red), Cu (cyan) and H (light grey). Guest molecules are omitted for clarity. **c**, **g**, Pore representation of DUT-49*op* (**c**) and DUT-49*cp* (**g**) along the [110] axis as natural tilings of the **nbo** topology net (the copper paddle wheels forming the (4,4)-connected network structure of NbO). Pores are coloured as follows: cuboctahedral MOP cavity (green), tetrahedral cavity (yellow) and octahedral cavity (orange). **d**, Evolution of pore sizes and free pore volume during contraction from DUT-49*op* to DUT-49*cp*. **h**, Evolution of density and accessible geometric surface area. Details of the simulation of intermediate structures, free pore volume, accessible surface area and pore sizes are given in Supplementary Fig. 40.

23.9 Å to 7.8 Å, resulting in an enormous overall pore volume reduction of 61% (see also visualization in Supplementary Video 2).

During desorption of methane at 111 K, two gradual phase transitions from DUT-49*op* to the intermediate-pore structure DUT-49*ip* ($V = 94{,}457$ Å^3, $a = 45.54$ Å, $\rho = 0.332\ \mathrm{g\ cm^{-3}}$) in the pressure range 30–20 kPa and from DUT-49*ip* to DUT-49*cp* at pressures lower than 20 kPa were observed, resulting in a wide hysteresis. Remarkably, during desorption at 111 K the framework does not switch back to the open form even at very low pressures (Supplementary Fig. 6). However, transformation to DUT-49*op* can be achieved by heating at a constant methane pressure of 100 kPa from 111 K to 298 K followed by evacuation (Supplementary Figs 7 and 9). *In situ* PXRD/adsorption experiments of *n*-butane at 298 K show DUT-49*op* to DUT-49*cp* transitions similar to those observed for methane adsorption at 111 K (Supplementary Fig. 32).

We used grand canonical Monte Carlo simulations performed for methane at 111 K in both DUT-49*op* and DUT-49*cp* to examine the microscopic adsorption mechanism. The experimental adsorption isotherm is precisely reproduced by simulating two adsorption regimes, starting with pore filling of DUT-49*op* up to 10 kPa, but continued adsorption in the contracted DUT-49*cp* (Fig. 4b, analogous observation for *n*-butane at 298 K; Supplementary Fig. 41). Methane initially occupies the smaller MOP cavities before gradually travelling over the tetrahedral and octahedral cages of DUT-49*op* with increasing pressure. After contraction above 11 kPa, the entire available space of the pores is occupied by the molecules (Fig. 4c). Indeed, this scenario strongly suggests that the filling of the mesopores triggers the structure contraction responsible for NGA.

Further analysis by quantum chemistry calculations using density functional theory showed that guest-molecule-free DUT-49*cp* is energetically substantially destabilized ($\Delta E = 91\ \mathrm{kJ\ mol^{-1}}$ per linker molecule) compared to DUT-49*op* owing to the highly strained organic ligand (Fig. 3a, e). Upon adsorption, this energy difference is overcome by the higher affinity of methane for the contracted-pore structure because filling the much smaller pores of DUT-49*cp* offers energetic benefits. Given the adsorption enthalpies of DUT-49*cp* and DUT-49*op* ($|\Delta H_{\mathrm{ads}}| \approx 17\ \mathrm{kJ\ mol^{-1}}$ and $10\ \mathrm{kJ\ mol^{-1}}$, respectively) (Supplementary Fig. 44 and Supplementary Table 13), the difference in adsorption enthalpy in the transition region, $\Delta\Delta H_{\mathrm{ads}} = n_{\mathrm{ads}}(cp) \cdot |\Delta H_{\mathrm{ads}}(op) - \Delta H_{\mathrm{ads}}(cp)| \approx 130\ \mathrm{kJ\ mol^{-1}}$ (Supplementary Equation (8)), is comparable in magnitude to ΔE, which suggests that adsorption compensates for the energy penalty of the structural transition (Supplementary Table 15). Analysis of the elastic properties of DUT-49*op* completes this picture: although the bulk modulus of 8.7 GPa is in the usual range for MOFs[28], the minimal shear modulus of the structure is relatively low at 1.5 GPa, with a strong nonlinearity showing a soft deformation mode that can be triggered by adsorption.

To summarize, in NGA a highly overloaded metastable state is created during gas adsorption in a hierarchical pore structure resulting in a spontaneous gas release and structural relaxation when the energy barrier is overcome. The result is a sudden reduction of porosity through network deformation triggered by adsorption-induced stress and the subsequent release of previously adsorbed gas[29]. Extended equilibration times of up to several hours (Supplementary Fig. 14) show that this phenomenon is not caused by inadequate equilibration of the system and indicate the presence of long-lived metastable states, possibly due to the vast extent of deformation and crossover of pore sizes (Fig. 3d), compared with the well known, purely microporous 'breathing' (that is, flexible or switchable) systems such as MIL-53[21]. This implies the internal reshuffling of molecules in DUT-49 from rigid MOP pores into contracted octahedral voids. The temperature dependence of NGA supports this thesis: the adsorption of methane at 91 K, 111 K, 101 K and 121 K (Fig. 4a, d) and of *n*-butane at 273–308 K (Supplementary Fig. 10) even shows a slight increase in $|\Delta n_{\mathrm{NGA}}|$ with

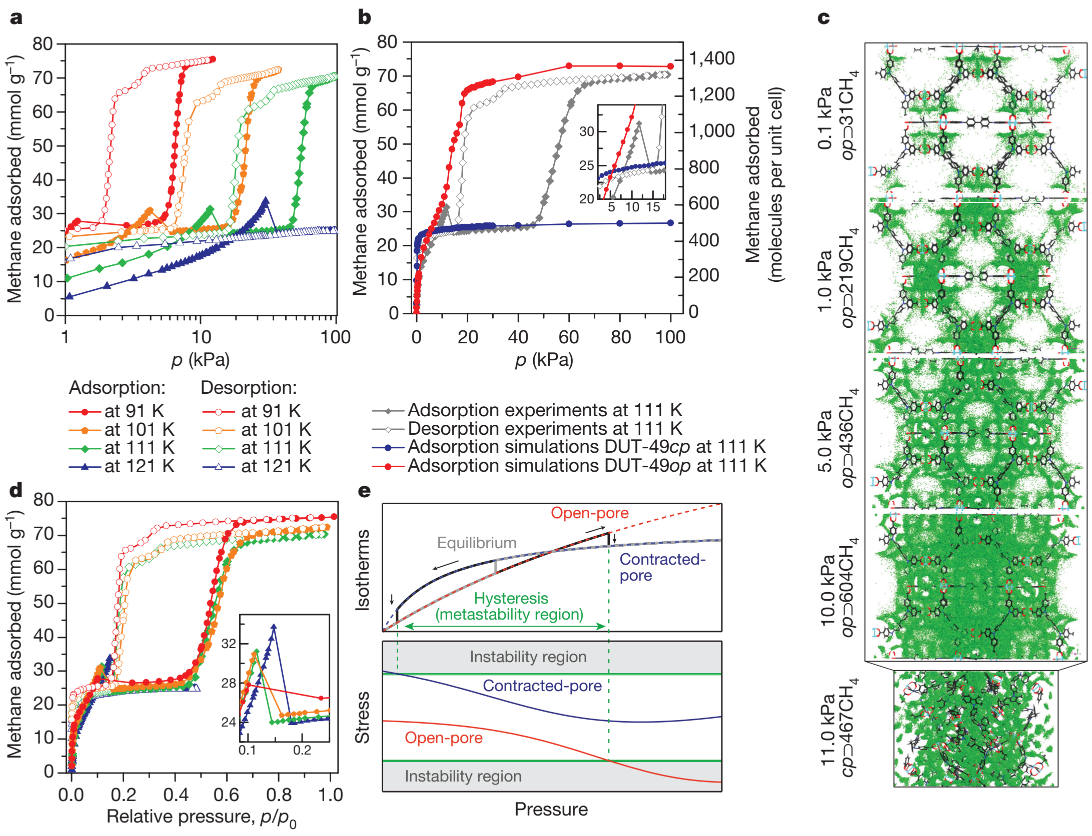

Figure 4 | Temperature-dependent methane adsorption and simulations. a, **d**, Methane adsorption isotherms at different temperatures. The inset in **d** shows an enlarged NGA region of the isotherm. **b**, Experimental (grey) and simulated methane sorption isotherm at 111 K based on the crystal structures of DUT-49*op* (red) and DUT-49*cp* (blue); the inset shows an enlarged NGA region of the isotherm. **c**, Maps of the occupied positions of methane (green) in 1,000 equilibrated frames for a given pressure for DUT-49*op* and at the transition pressure (11 kPa) of DUT-49*cp* (bottom frame). Atoms are coloured as in Fig. 3. **e**, Schematic representation of stress-based model for adsorption-induced structural transformation[29]: equilibrium transition (grey line), metastable transition (black arrows), open-pore phase (red line), contracted-pore phase (blue line); arrows indicate the transition observed for DUT-49.

temperature up to 9.87 mmol of methane per gram of MOF at 121 K. However, the pore contraction mechanism is maintained, as reflected by the almost identical relative pressure ($p/p_0 = 0.1$–0.15) (where p_0 is the saturation pressure of the bulk fluid) at which NGA is observed (Supplementary Figs 27 and 30). This suggests that filling of the mesopores induces the contraction (Fig. 4a, c).

To our knowledge, the phenomenon of NGA in MOFs has not been reported before. The rare metastable cation complexes in zeolite materials could be considered to have analogous properties[30]. Besides the fundamental interest of this phenomenon, there are many possible technological applications. These porous solids could enable the design of threshold-sensitive micropneumatic devices, stimuli-responsive self-propelling systems or mechanical actuators responding selectively to changes in the environment, and capable of transforming a large amount of latent strain into pressure.

Received 3 October 2015; accepted 16 February 2016.

1. de Vos, R. M. & Verweij, H. High-selectivity, high-flux silica membranes for gas separation. *Science* **279,** 1710–1711 (1998).
2. Nenoff, T. M. Hydrogen purification: MOF membranes put to the test. *Nature Chem.* **7,** 377–378 (2015).
3. McDonald, T. M. *et al.* Cooperative insertion of CO$_2$ in diamine-appended metal-organic frameworks. *Nature* **519,** 303–308 (2015).
4. Barea, E., Montoro, C. & Navarro, J. A. R. Toxic gas removal—metal-organic frameworks for the capture and degradation of toxic gases and vapours. *Chem. Soc. Rev.* **43,** 5419–5430 (2014).
5. Furukawa, H. *et al.* Water adsorption in porous metal–organic frameworks and related materials. *J. Am. Chem. Soc.* **136,** 4369–4381 (2014).
6. Kitagawa, S., Kitaura, R. & Noro, S.-i. Functional porous coordination polymers. *Angew. Chem. Int. Ed.* **43,** 2334–2375 (2004).
7. Furukawa, H., Cordova, K. E., O'Keeffe, M. & Yaghi, O. M. The chemistry and applications of metal-organic frameworks. *Science* **341,** http://dx.doi.org/10.1126/science.1230444 (2013).
8. Nugent, P. *et al.* Porous materials with optimal adsorption thermodynamics and kinetics for CO$_2$ separation. *Nature* **495,** 80–84 (2013).
9. Horike, S., Shimomura, S. & Kitagawa, S. Soft porous crystals. *Nature Chem.* **1,** 695–704 (2009).
10. Schneemann, A. *et al.* Flexible metal-organic frameworks. *Chem. Soc. Rev.* **43,** 6062–6096 (2014).
11. Matsuda, R. Materials chemistry: selectivity from flexibility. *Nature* **509,** 434–435 (2014).
12. Sato, H. *et al.* Self-accelerating CO sorption in a soft nanoporous crystal. *Science* **343,** 167–170 (2014).
13. Takashima, Y. *et al.* Molecular decoding using luminescence from an entangled porous framework. *Nature Commun.* **2,** 168 (2011).
14. Yang, S. *et al.* A partially interpenetrated metal–organic framework for selective hysteretic sorption of carbon dioxide. *Nature Mater.* **11,** 710–716 (2012).
15. Martinek, C. & Hummel, F. A. Linear thermal expansion of three tungstates. *J. Am. Ceram. Soc.* **51,** 227–228 (1968).
16. Takenaka, K. Negative thermal expansion materials: technological key for control of thermal expansion. *Sci. Technol. Adv. Mater.* **13,** 013001 (2012).
17. Shelby, R. A., Smith, D. R. & Schultz, S. Experimental verification of a negative index of refraction. *Science* **292,** 77–79 (2001).
18. Nicolaou, Z. G. & Motter, A. E. Mechanical metamaterials with negative compressibility transitions. *Nature Mater.* **11,** 608–613 (2012).
19. Fairen-Jimenez, D. *et al.* Opening the gate: framework flexibility in ZIF-8 explored by experiments and simulations. *J. Am. Chem. Soc.* **133,** 8900–8902 (2011).
20. Kondo, A. *et al.* Novel expansion/shrinkage modulation of 2D layered MOF triggered by clathrate formation with CO$_2$ molecules. *Nano Lett.* **6,** 2581–2584 (2006).
21. Serre, C. *et al.* An explanation for the very large breathing effect of a metal–organic framework during CO$_2$ adsorption. *Adv. Mater.* **19,** 2246–2251 (2007).
22. Férey, G. & Serre, C. Large breathing effects in three-dimensional porous hybrid matter: facts, analyses, rules and consequences. *Chem. Soc. Rev.* **38,** 1380–1399 (2009).

23. Salles, F. *et al.* Multistep N_2 breathing in the metal—organic framework Co(1,4-benzenedipyrazolate). *J. Am. Chem. Soc.* **132,** 13782–13788 (2010).
24. Thommes, M. *et al.* Physisorption of gases, with special reference to the evaluation of surface area and pore size distribution (IUPAC Technical Report). *Pure Appl. Chem.* **87,** 1051–1069 (2015).
25. Stoeck, U., Krause, S., Bon, V., Senkovska, I. & Kaskel, S. A highly porous metal-organic framework, constructed from a cuboctahedral super-molecular building block, with exceptionally high methane uptake. *Chem. Commun.* **48,** 10841–10843 (2012).
26. Traa, Y. & Weitkamp, J. in *Handbook of Porous Solids* (eds, Schüth, F., Sing, K. S. W. & Weitkamp, J.) 1015–1057 (Wiley, 2008).
27. Bon, V. *et al.* In situ monitoring of structural changes during the adsorption on flexible porous coordination polymers by X-ray powder diffraction: instrumentation and experimental results. *Micropor. Mesopor. Mater.* **188,** 190–195 (2014).
28. Tan, J. C. & Cheetham, A. K. Mechanical properties of hybrid inorganic–organic framework materials: establishing fundamental structure–property relationships. *Chem. Soc. Rev.* **40,** 1059–1080 (2011).
29. Neimark, A. V., Coudert, F.-X., Boutin, A. & Fuchs, A. H. Stress-based model for the breathing of metal–organic frameworks. *J. Phys. Chem. Lett.* **1,** 445–449 (2010).
30. Riekert, L. Instability of sorption complexes in synthetic faujasites. *J. Phys. Chem.* **73,** 4384–4386 (1969).

Supplementary Information is available in the online version of the paper.

Acknowledgements V.B. thanks the German Federal Ministry for education and research (project BMBF number 05K13OD3). S. Krause, V.B., I.S. and S. Kaskel thank the Helmholtz-Zentrum Berlin for financial support and allocation of synchrotron radiation beam time at the KMC-2 beamline. F.-X.C. thanks GENCI (grant number x2015087069) for access to High-Performance Computing resources. G.M. thanks Institut Universitaire de France for its support. We thank U. Koch for scanning electron microscope images, as well as L. Sarkisov and A. Fuchs for discussions.

Author Contributions S. Krause and U.S. synthesized and activated the material investigated; S. Krause, V.B., I.S. and S. Kaskel conducted and interpreted volumetric and gravimetric sorption experiments. S. Krause, V.B., D.W. and D.M.T. conducted the *in situ* PXRD investigations. S. Krause V.B., D.W. and S.Z. conducted the *in situ* EXAFS investigations. V.B. solved the crystal structure and performed structure modelling. S. Krause performed filming and animation of the structural transitions. F.-X.C. performed quantum mechanical calculations. G.M. and R.S.P. performed the grand canonical Monte Carlo simulations of adsorption. S. Krause, V.B., I.S., F.-X.C., G.M. and S. Kaskel wrote the manuscript.

Author Information The following crystal structures are available free of charge from the Cambridge Crystallographic Data Centre under reference numbers CCDC-1413081, CCDC-1413083, CCDC-1413082 and CCDC-1413084, respectively: DUT-49*op* in vacuum at 111 K; DUT-49*cp*$\supset$432CH_4 (where $\supset$ indicates the number of methane molecules per unit cell) at a relative pressure of 0.28 for methane at 111 K during adsorption; DUT-49*op*$\supset$1,344CH_4 at a relative pressure of 0.97 for methane at 111 K during adsorption; and DUT-49*ip*$\supset$1,176CH_4 at a relative pressure of 0.25 for methane at 111 K during desorption. Reprints and permissions information is available at www.nature.com/reprints. The authors declare no competing financial interests. Readers are welcome to comment on the online version of the paper. Correspondence and requests for materials should be addressed to S. Kaskel (stefan.kaskel@chemie.tu-dresden.de).